NEUTRINO ASTROPHYSICS

Evidence for neutrino emission from the nearby active galaxy NGC 1068

IceCube Collaboration*†

A supermassive black hole, obscured by cosmic dust, powers the nearby active galaxy NGC 1068. Neutrinos, which rarely interact with matter, could provide information on the galaxy's active core. We searched for neutrino emission from astrophysical objects using data recorded with the IceCube neutrino detector between 2011 and 2020. The positions of 110 known gamma-ray sources were individually searched for neutrino detections above atmospheric and cosmic backgrounds. We found that NGC 1068 has an excess of 79^{+22}_{-20} neutrinos at tera–electron volt energies, with a global significance of 4.2σ, which we interpret as associated with the active galaxy. The flux of high-energy neutrinos that we measured from NGC 1068 is more than an order of magnitude higher than the upper limit on emissions of tera–electron volt gamma rays from this source.

Observations of high-energy cosmic rays (protons and atomic nuclei from space), up to 10^{19} to 10^{20} eV (*1*–*3*), have demonstrated that powerful cosmic particle accelerators must exist, but their nature and location remain unknown. Interstellar magnetic fields change the direction of charged cosmic particles during their propagation to Earth, concealing their sources. High-energy photons and neutrinos are not deflected, so they could be used to locate the cosmic accelerators. Both travel along straight paths and are produced wherever cosmic rays interact with ambient matter or light, in or near the acceleration sites (*4*, *5*). Depending on the environment in which these interactions occur, gamma rays could rapidly lose energy through several processes, including pair-production in interactions with lower-energy photons. Above tera–electron volt energies, gamma rays are strongly absorbed over cosmological distances through interactions with the extragalactic background light and the cosmic microwave background (*6*). Neutrinos are not affected by intergalactic absorption, so they could potentially be used to probe tera–electron volt cosmic accelerators.

Active galaxies, those that host an active galactic nucleus (AGN) (*7*), are characterized by a very bright central region powered by the accretion of material onto a supermassive black hole (SMBH). The accretion flow of matter into the SMBH is usually surrounded by an obscuring, dusty torus, causing the observable characteristics of an AGN to depend on the viewing angle from Earth. For example, Seyfert II galaxies (*8*) are thought to be viewed edge on, with the line of sight passing directly through the obscuring torus (*9*). In some cases, the AGN can launch a strong, narrow jet of accelerated plasma. If such a jet is oriented close to the line of sight, the AGN is observed as a blazar (*10*). AGNs are potential neutrino emitters (*11*, *12*); if a plasma jet is present, it might dominate the emission (*13*, *14*).

The IceCube Neutrino Observatory (*15*) is based at the Amundsen-Scott South Pole Station in Antarctica and has been operating since 2010. The observatory uses 1 km^3 of optically transparent glacial ice as a detection medium to measure Cherenkov light—ultraviolet and blue photons emitted by charged secondary particles traveling at a speed above the phase velocity of light in the ice. These relativistic (close to the speed of light) secondary particles are produced when neutrinos interact with nuclei in or near the instrument. A total of 5160 digital optical modules (DOMs) are installed on 86 vertical cables (strings), spaced 125 m apart to form a three-dimensional array in the ice. Each DOM records the number of induced photoelectrons (charges) as a function of time.

The measured flux of astrophysical neutrinos (*16*) is largely isotropic, equally distributed among neutrino flavors, and can be described by a single power-law energy distribution that extends from ~10 TeV to peta–electron volt energies (*17*, *18*). A specific source of high-energy cosmic neutrinos was reported after the spatial and temporal coincidence of a high-energy IceCube neutrino (*19*) with a gamma-ray flaring blazar, TXS 0506+056 (*20*–*22*). TXS 0506+056 contains a typical accretion disk and a dusty torus, which emits high-energy radiation and, possibly, cosmic rays (*22*). Neutrinos detected using IceCube were correlated with a catalog of 110 known gamma-ray emitters, with a significance of 3.3σ (*23*). The individual sources that made the largest contribution to the total significance of that catalog were the active galaxy NGC 1068 and the blazars TXS 0506+056, PKS 1424+240, and GB6 J1542+6129. The significance of the neutrino excess from the direction of NGC 1068 was reported as 2.9σ, which is insufficient to claim a detection (*23*).

Searching for point-like neutrino emission

We analyzed data collected with IceCube between 13 May 2011 and 29 May 2020. This period begins with the installation of the full 86-string detector configuration. Previous searches for cosmic neutrino sources (*23*) included data collected with the incomplete detector with fewer strings going back to 2008 and the full detector up to the spring of 2018. We only used the full detector data because our methods depend on uniformly processed data. The IceCube dataset we used (*24*) has consistent selection criteria (*25*). We reprocessed these data uniformly to remove data sample fragmentation, align different data-taking conditions and calibrations, and improve event reconstructions

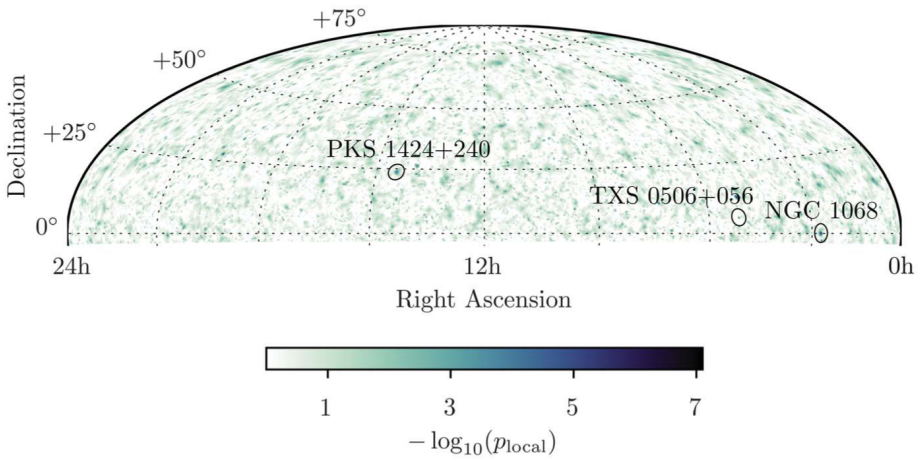

Fig. 1. Sky map of the scan for point sources in the Northern Hemisphere. The color scale indicates the logarithm of the local *P* value (P_{local}) obtained from our maximum likelihood analysis, evaluated (with the spectral index as a free parameter) at each location in the sky. The map is shown in equatorial coordinates on a Hammer-Aitoff projection. The black circles indicate the three most significant objects in the source list search, which are labeled. The circle around NGC 1068 contains the most significant location in the Northern Hemisphere, shown in higher resolution in Fig. 2A.

*Corresponding authors: analysis@icecube.wisc.edu; F. Halzen (francis.halzen@icecube.wisc.edu)
†IceCube Collaboration authors and affiliations are listed in the supplementary materials.

(*26*). We applied the directional track reconstruction method SplineReco (*26*, *27*, *28*) to all events in our dataset (*26*). We incorporated additional calibration information in the extraction of the charges at each DOM and in the corresponding arrival times of Cherenkov photons. Compared with previous work (*23*), this introduces small changes in the reconstructed event energies and some reconstructed event directions (*26*). To ensure a uniform detector response, the DOMs of the DeepCore subarray, intended to study ≲100-GeV neutrinos, were excluded (*25*). Our resulting dataset, which is optimized for track-like events induced by muon (anti-)neutrinos $\left[{}^{(-)}_{\nu_\mu}\right]$, has a total exposure time of 3186 days.

We restricted our searches to the Northern Hemisphere from declination $\delta = -3°$ to 81°, where IceCube is most sensitive to astrophysical sources. IceCube uses Earth as a passive cosmic muon shield and as a target material for neutrinos. Hence, by selecting only upward-going events, we reduced the atmospheric muon background, which contributes <0.3% to our final event sample (*25*). Declinations higher than 81° are excluded because low-energy events from those directions are closely aligned with the strings of IceCube, complicating our distinction between the signal and background (*26*). The resulting loss of sky coverage is <1%.

A total of ~670,000 neutrino-induced muon tracks pass the final event selection criteria (*25*). However, only a small fraction of these events originate from neutrinos produced in astrophysical sources. Most arise from the decay of particles (specifically mesons) that are produced in the interaction of cosmic rays with nuclei in Earth's atmosphere. To discriminate neutrinos that originate from individual astrophysical sources from the background of atmospheric and diffuse astrophysical neutrinos, we used a maximum-likelihood method and likelihood ratio hypothesis testing, based on the estimated energy, direction, and angular uncertainty of each event (*26*). The median angular resolution of each neutrino arrival direction, composed of reconstruction uncertainty and the kinematic angle between the parent neutrino and the muon, is 1.2° at 1 TeV, 0.4° at 100 TeV, and 0.3° at 1 PeV. We assume any point source emits a neutrino flux $\Phi_{\nu_\mu+\bar{\nu}_\mu}$ described by a generalized power-law energy spectrum, $\Phi_{\nu_\mu+\bar{\nu}_\mu}(E_\nu) = \Phi_0 \cdot (E_\nu/E_0)^{-\gamma}$, with normalization energy $E_0 = 1$ TeV, where E_ν is the neutrino energy and the spectral index γ and the flux normalization Φ_0 are free parameters (*26*). This corresponds to two correlated model parameters that we express as a pair (μ_{ns}, γ), where μ_{ns} is the mean number of astrophysical neutrino events associated with a given point in the sky. Using the energy- and declination-dependent effective area of the detector and assuming a spectral index γ, μ_{ns} can be directly converted to Φ_0 (*26*). Hence, the tuple of μ_{ns} and γ fully determines the flux of muon neutrinos, $\Phi_{\nu_\mu+\bar{\nu}_\mu}$, at any given energy.

We performed three different searches (*26*). The first search consists of three discrete scans of the Northern Hemisphere to identify the location of the most statistically significant excesses of high-energy neutrino events. These scans use three different hypotheses for the spectral index: γ as a free parameter, γ fixed to 2.0, and γ fixed to 2.5. The other two searches use a list of 110 preselected astronomical objects, all located in the Northern Hemisphere: The second search is for the most significant candidate neutrino source in the list, whereas the third search consists of a binomial test to evaluate the significance of observing an excess of k sources with local P values below or equal to a chosen threshold, with k being an index from 1 to 110. The binomial test is repeated under the same three spectral index hypotheses as the sky scan.

All analysis methods, including the selection of the hypotheses to be tested, were formulated a priori. The performance of each method was evaluated using simulations and randomized experimental data (*26*). The local P values are determined as the fraction of background-only simulations that yield a test statistic greater than (or equal to) the test statistic obtained from the experimental data. The global P values are determined from the smallest local P value after correcting for testing multiple locations (the look-elsewhere effect) (*26*). We use this global value to assess the evidence that the data provide against a background-only null hypothesis (that the data consist purely of atmospheric background and isotropic cosmic neutrinos).

Table 1. Summary of final *P* values. For each of the three tests performed, we report the most significant local and global P values.

Test type	Pretrial P value, P_{local} (local significance)	Posttrial P value, P_{global} (global significance)
Northern Hemisphere scan	5.0×10^{-8} (5.3σ)	2.2×10^{-2} (2.0σ)
List of candidate sources, single test	1.0×10^{-7} (5.2σ)	1.1×10^{-5} (4.2σ)
List of candidate sources, binomial test	4.6×10^{-6} (4.4σ)	3.4×10^{-4} (3.4σ)

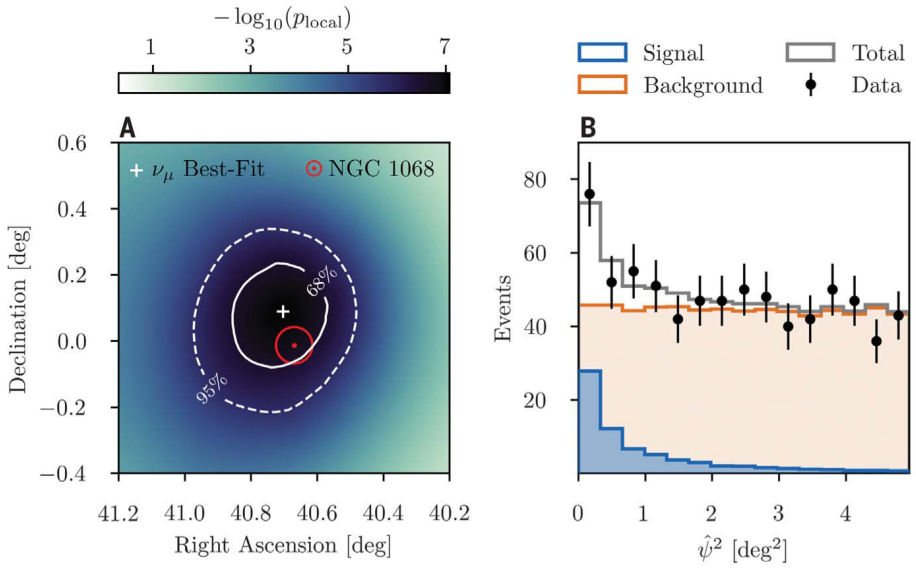

Fig. 2. High-resolution scan around the most significant location. (**A**) High-resolution scan around the most significant location marked by a white cross, with contours showing its 68% (solid) and 95% (dashed) confidence regions. The red dot shows the position of NGC 1068, and the red circle is its angular size in the optical wavelength (*61*). (**B**) The distribution of the squared angular distance, $\hat{\psi}^2$, between NGC 1068 and the reconstructed event directions. We estimated the background (orange) and the signal (blue) from Monte Carlo simulations, assuming the best-fitting spectrum at the position of NGC 1068. The superposition of both components is shown in gray and the data in black. This representation of the result ignores the energy and angular uncertainty of the events.

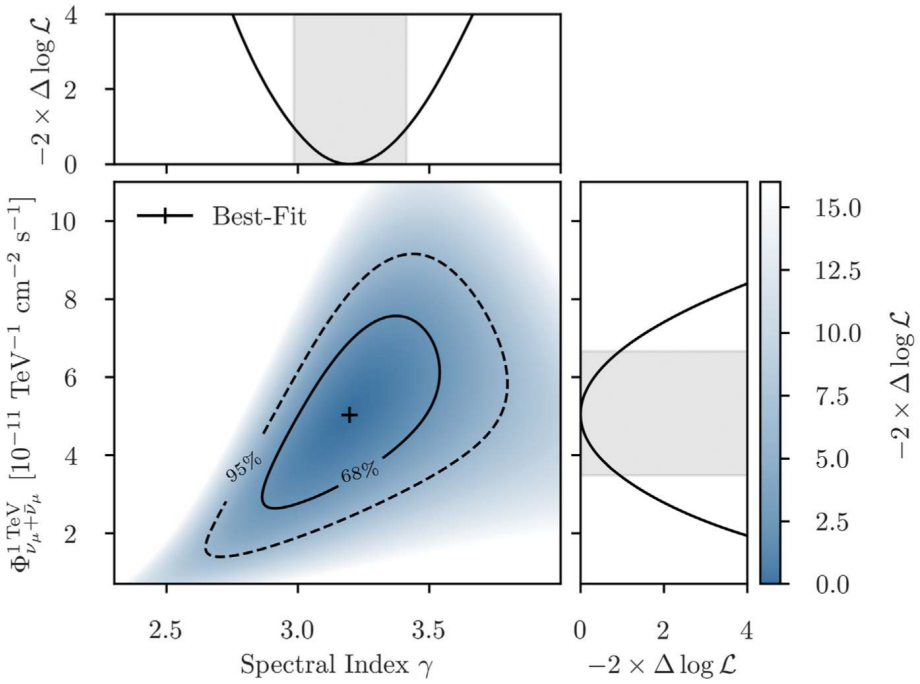

Fig. 3. Source parameters of NGC 1068. The best-fitting flux values are shown as the black cross, with the solid and dashed contours representing the 68% and 95% confidence levels, respectively. These were derived from Wilks' theorem—i.e., by using the log-likelihood ratio (color scale), $-2\Delta \log \mathcal{L}$, between any fixed values for the two flux parameters $\left(\gamma, \Phi^{1\,\mathrm{TeV}}_{\nu_\mu+\bar{\nu}_\mu}\right)$ and the overall best-fitting point marked by the cross. The side panels show the corresponding one-dimensional projections (profile likelihoods) as black solid lines, with the gray shaded areas showing the one-dimensional 68% confidence levels (as reported in the text). All contours include only statistical uncertainties.

The discrete scan of the sky maximizes the signal and background likelihood functions at each point on an ~(0.2° × 0.2°) grid, determining the local value of the test statistic, the best-fitting value of the mean number of astrophysical neutrino events $(\hat{\mu}_{\mathrm{ns}})$, and the mean spectral index $(\hat{\gamma})$. The scan is repeated with fixed spectral indices $\gamma = 2.0$ and $\gamma = 2.5$ to reduce the impact of background fluctuations, which arise from atmospheric neutrinos. The atmospheric spectrum, produced by the decay of charged pions and kaons as well as the muons produced when pions and kaons decay, follows a power law with $\gamma \approx 3.7$ (*29*), and thus those fluctuations typically yield $\hat{\gamma} \gtrsim 3$. Fixing the spectral index therefore increases the sensitivity to astrophysical sources with $\gamma < 3$. For the 20 most significant locations in each of the three searches, we scan the 1.5° × 1.5° vicinity using increased resolution of ~(0.03° × 0.03°) on a square grid. We find the most significant location identified in the first scan (with free spectral index) at right ascension 40.69° and declination 0.09° (J2000 equinox) with $\hat{\gamma} = 3.2$ and $\hat{\mu}_{\mathrm{ns}} = 81$.

Sky scan search

The full sky map of the discrete scan is shown in Fig. 1. At the most significant location, the local *P* value is 5×10^{-8}, which corresponds to a local significance of 5.3σ. After including a penalty for the multiple tests performed—i.e., how likely it is to observe an equal or larger significance when scanning many independent sky positions under the three spectral index hypotheses (*26*)—the global *P* value corresponds (*26*) to 2.0σ and is therefore not significant without additional prior information. The high-resolution scan around the most significant location is shown in Fig. 2A.

We searched a posteriori for astrophysical counterparts in close proximity to the direction of the five most significant locations in each of the three sky maps. The nearby active galaxy NGC 4151 (*8*) is located at ~0.18° from the fourth most significant location in the map obtained with $\gamma = 2.5$.

Source list search

Searching the entire Northern Hemisphere requires a strong numerical penalty because of testing multiple locations. This trials factor can be reduced by restricting the search to a list of a priori selected positions based, for example, on known gamma-ray emission (*30*). To avoid confirmation bias, we maintain the previous selection method (*23*), which was adopted before there was any indication for neutrino emission from NGC 1068 (*31*). This approach identified a total of 110 objects within the declination range we analyzed, $-3° \leq \delta \leq 81°$. The number of objects in the list was chosen such that a local 5σ detection corresponds to a global detection >4σ after accounting for the number of trials. The 110 astronomical objects were selected from the gamma-ray flux weighted by the IceCube sensitivity. Using the gamma-ray flux above 1 GeV (*32*), the list contains 95 blazars, 5 AGNs, and 9 other types of galaxies. One galactic source is added because of its tera–electron volt gamma-ray emission (*26*, *33*). We do not assume or require any relationship between the observed gamma-ray flux and the hypothesized neutrino flux during our hypothesis testing (*26*).

Of the 110 astronomical objects tested, NGC 1068 is the most significant with a local *P* value of 1×10^{-7} (5.2σ); it has best-fitting values of spectral index $\hat{\gamma} = 3.2^{+0.2}_{-0.2}$ and mean number of signal events $\hat{\mu}_{\mathrm{ns}} = 79^{+22}_{-20}$. NGC 1068 is contained within the 68% confidence region around the most significant location in the sky scan, offset by 0.11° (less than the directional uncertainty), consistent with neutrino emission from NGC 1068 (Fig. 2). After correcting for having tested the 110 sources in the catalog, the global *P* value for NGC 1068 is 1.1×10^{-5}, corresponding to a significance of 4.2σ.

Binomial test

We performed a binomial test to investigate how likely it is to find an excess of *k* sources from the catalog with local *P* values below or equal to a threshold (*26*), as defined a priori. By scanning the *P* value threshold, we find the smallest background probability for an excess of $k = 3$ sources, under the free spectral index hypothesis, with local *P* values $\leq 4.6 \times 10^{-6}$. This is equivalent to a local significance of 3.7σ, a small increase from the previous search (*23*). After correcting for having tested three different spectral index hypotheses, we obtain a posttrial significance of 3.4σ for the binomial test. Besides NGC 1068, the other two objects contributing to the excess are the blazars PKS 1424+240 and TXS 0506+056 (Fig. 1), for which we found potential neutrino emission with local significances of 3.7σ and 3.5σ, respectively. This significance of TXS 0506+056 relates to a time-integrated signal over the duration of our dataset, whereas previous analyses have found evidence for transient emission (*20*, *21*, *34*). A search for transient emission has a lower effective background than our time-integrated searches. The total number of contributing candidate sources ($k = 3$) in the binomal test is lower than the four previously reported (*23*). Although the local significance of PKS 1424+240 increased from 3.0σ to 3.7σ, the local significance of GB6 J1542+61 decreased from 2.9σ to 2.2σ, falling below the threshold corresponding to the best-fitting binomial *P* value. The results of all three searches (*26*) are summarized in Table 1.

Neutrino emission from NGC 1068

The high-resolution scan around the most significant location in the Northern Hemisphere is shown in Fig. 2A, with NGC 1068 located inside the 68% confidence region. The position of NGC 1068 produced $\hat{\mu}_{ns} = 79^{+22}_{-20}$ more events than expected from the atmospheric and diffuse astrophysical neutrino backgrounds. Figure 2B shows the distribution of the angular separation of these events from NGC 1068. Among the 79 most contributing events, 63 were included in a previous analysis (*23*). The systematic uncertainty on $\hat{\mu}_{ns}$ is ~2 events (*26*). The measured spectral index is $\hat{\gamma} = 3.2^{+0.2}_{-0.2}$ with an estimated systematic uncertainty of ±0.07 (*26*), consistent with previous results (*23*). We estimate these systematic uncertainties by analyzing simulated data, assuming a source with flux equal to the one measured for NGC 1068 but varying assumptions about the detector response (*26*). Systematic uncertainties arise mainly from the modeling of the photon propagation in the glacial ice—e.g., scattering and absorption—and the efficiency with which photons are detected by the IceCube optical modules. Systematic uncertainties are smaller than statistical uncertainties for directional track reconstructions (*26*) but have a nonnegligible effect on the energy reconstructions.

The properties of the source spectrum are shown in Fig. 3, which shows the likelihood as a function of the model parameters (Φ_0, γ) evaluated at the coordinates of NGC 1068. The conversion of $\hat{\mu}_{ns}$ to the flux Φ_0 accounts for the contribution from tau neutrino interactions (which produce muons) assuming an equal neutrino flavor ratio. The best-fitting flux averaged over the data-taking period, at a neutrino energy of 1 TeV, is $\Phi^{1\mathrm{TeV}}_{\nu_\mu+\bar{\nu}_\mu} = (5.0 \pm 1.5_{\mathrm{stat}} \pm 0.6_{\mathrm{sys}}) \times 10^{-11}\,\mathrm{TeV}^{-1}\,\mathrm{cm}^{-2}\mathrm{s}^{-1}$. This systematic uncertainty was estimated by varying the flux normalization under different ice and detector properties, such that we reproduce the observed values of $\hat{\gamma}$ and $\hat{\mu}_{ns}$ in the median case.

Our analysis assumed that the spectrum follows an unbroken power law over the entire energy range of the dataset. However, our results show that the main contribution to the excess (and thus the measured spectral index and flux normalization) comes from neutrinos in an energy range from 1.5 to 15 TeV, which contributes 68% to the total test statistic. Outside this energy range, the data do not strongly constrain the inferred flux properties. Our results strengthen the suggestion (*23*) that NGC 1068 could be a neutrino source; we find a higher statistical significance for this result (4.2σ versus 2.9σ).

Incrementally removing the most contributing neutrino events one by one from the vicinity of NGC 1068 shows that the excess persists, which indicates that it is not dominated by one or a few single events but is the result of an accumulation of neutrinos (*26*). We visually inspected all neutrino events contributing to the excess from NGC 1068, finding typical, well-reconstructed, horizontal, and approximately tera–electron volt–energy tracks with no sign of unexpected contamination or anomalies (*26*). Out of the 20 events contributing the most to the test statistic, 19 were included in the previous analysis (*23*). Although the location is therefore dominated by the same neutrinos, the

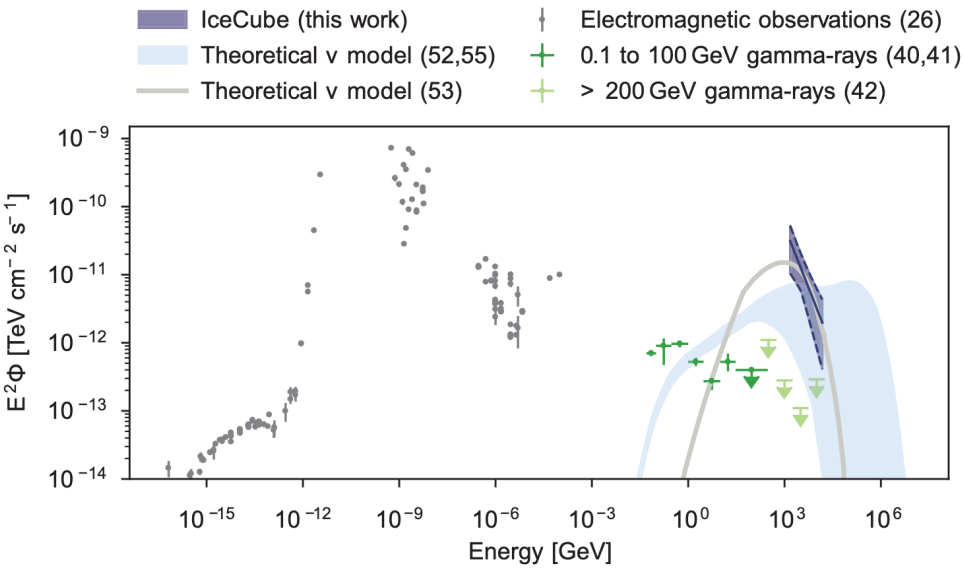

Fig. 4. Multimessenger spectral energy distribution of NGC 1068. Gray points show multifrequency observations (data sources listed in table S1). Dark and light green points indicate gamma-ray observations at 0.1 to 100 GeV (*40*, *41*) and >200 GeV (*42*), respectively. Arrows indicate upper limits, and error bars are 1σ confidence intervals. The solid, dark blue line shows our best-fitting neutrino spectrum with the dark blue shaded region indicating the 95% confidence region. We restrict this spectrum to the range between 1.5 and 15 TeV, where the flux measurement is well constrained (*26*). Two theoretical predictions are shown for comparison: The light blue shaded region and the gray line show the NGC 1068 neutrino emission models from (*52*, *55*) and (*53*), respectively. The shaded region covers possible values of the gyrofactor $30 \le \eta_g \le 10^4$ used to describe uncertainty in the efficiency of the underlying particle acceleration (*55*). All fluxes Φ are multiplied by the energy squared E^2.

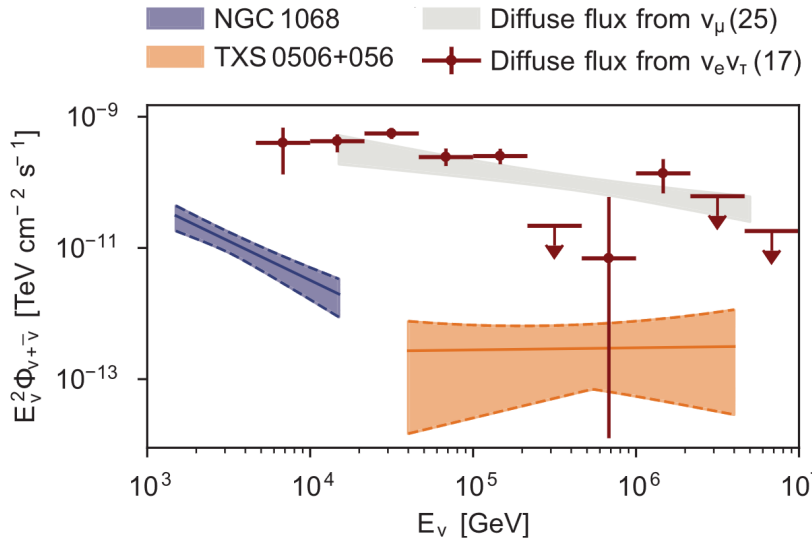

Fig. 5. Comparison of point-source fluxes with the total diffuse astrophysical neutrino flux. Fluxes for NGC 1068 (blue line, this work), TXS 0506+056 (orange line, this work), and the diffuse neutrino background [brown data points and gray band (*17*, *25*)] are given for a single flavor of neutrinos and antineutrinos. All fluxes $\Phi_{\nu+\bar{\nu}}$ are multiplied by the neutrino energy squared E^2_ν. For the conversion of the diffuse astrophysical flux measured from the $\nu_e\nu_\tau$ channel (*17*), we assume an equal flavor ratio. Shaded regions and dashed lines indicate 68% confidence intervals. Downward arrows are 68% upper limits.

differences in the data processing modify their contribution to the likelihood function. These changes are small but consistently cause the reconstructed neutrinos to align more closely with the direction of NGC 1068, thus strengthening the association (*26*).

Astrophysical interpretation

The flux we measured from the direction of NGC 1068 was 79^{+22}_{-20} muon-neutrino events over a period of 3186 days, corresponding to $\Phi^{1\,\mathrm{Tev}}_{\nu_\mu+\bar{\nu}_\mu} = (5.0 \pm 1.5_{\mathrm{stat}}) \times 10^{-11}$ TeV^{-1} cm^{-2}s^{-1}. If all neutrino flavors contribute equally, as expected for sources dominated by pion decay and neutrino oscillations over cosmic distances (*35*, *36*), the all-flavor flux is a factor of 3 higher. We adopt a distance of 14.4 Mpc for NGC 1068 (*37*), although values in the literature range from 10.3 ± 3 Mpc (*38*) to 16.5 Mpc (*39*). For comparison, assuming isotropic emission, this leads to a redshift-corrected equivalent neutrino luminosity L_ν, from 1.5 to 15 TeV and at 14.4 Mpc, of $L_\nu = (2.9 \pm 1.1_{\mathrm{stat}}) \times 10^{42}$ erg s^{-1}. This is higher than the equivalent gamma-ray luminosity of 1.6×10^{41} erg s^{-1} observed in the energy range 100 MeV to 100 GeV (*40*, *41*) and higher than the upper limits reported above 200 GeV (*42*) (Fig. 4).

High-energy neutrinos are generated in or near astronomical sources as decay products of charged mesons, which are themselves produced in proton-proton interactions (*4*), or interactions between protons and low-energy ambient radiation (*5*). Gamma rays are also produced in the same processes, through the decay of neutral mesons. Neutrinos escape the site without further interactions, whereas photons may experience additional interactions depending on the optical depth of the environment. Therefore, the connection between neutrinos and gamma rays is highly dependent on the astrophysical environment. NGC 1068 (*8*) is a nearby Seyfert II galaxy that hosts a Compton-thick AGN (*43*–*45*), has vigorous starburst activity (*46*, *47*) and outflows (*48*), and for these reasons has previously been discussed as a potential source of high-energy neutrinos (*49*–*51*). Neutrino emission models (*52*, *53*) have predicted the production of neutrinos and gamma rays within the heavily obscured environment around the NGC 1068 AGN (*49*, *54*). In those models, the SMBH in the AGN provides the acceleration conditions, with x-ray photons generated through photon Comptonization from the accretion disk in the hot plasma above the disk, called the corona, providing the conditions for the production of neutrinos and absorption of gamma rays. Figure 4 compares our neutrino flux measurement with the model predictions (*52*, *53*).

The evidence of neutrino emission from NGC 1068 suggests that AGNs could make a substantial contribution to the diffuse neutrino flux. Figure 5 compares the neutrino fluxes from the AGN NGC 1068 and the blazar TXS 0506+056 with the overall diffuse flux of astrophysical neutrinos. These two sources contribute ~1% of the total diffuse flux in their observed energy ranges. For NGC 1068, the observed energy range does not strongly overlap with the diffuse flux, and its best-fitting spectral index of $\hat{\gamma} = 3.2^{+0.2}_{-0.2}$ is higher than the diffuse flux with $\gamma = 2.53^{+0.07}_{-0.07}$ (*17*). Nonetheless, it is evident that the diffuse flux could contain additional bright and nearby sources, like NGC 1068, a large population of faint sources, or both. For example, the nearby Seyfert I galaxy NGC 4151 has previously been suggested as a potential neutrino source (*55*, *56*, *57*). Depending on the luminosity function and cosmological evolution, the contribution from many faint sources at large distances (redshift $z \gtrsim 1$) could be large (*58*, *59*).

We cannot characterize the underlying source population with so few known point sources. However, our observation of neutrino emission from NGC 1068 can place constraints on the density ρ of AGNs with similar or greater neutrino luminosity in the local Universe, independent of the precise emission process or processes. If there is one source within a spherical volume of radius 14.4 Mpc (*37*), the distance to NGC 1068, then $\rho \lesssim 10^{-4}$ Mpc^{-3}. This density estimate relies on the observation of a single source, which may or may not be representative of the population, so this is an upper limit. Simulations of populations with various luminosity functions (*60*) have an uncertainty of more than an order of magnitude. Nevertheless, given the differences in spectrum and distance between NGC 1068 and TXS 0506 +056, which is ~100 times farther away, we suggest that there are at least two populations of neutrino sources, which could differ in both density and luminosity by orders of magnitude.

We have observed evidence for neutrino emission from the active galaxy NGC 1068 at the 4.2σ level of significance, which we interpret as a signature of hadronic particle acceleration. The observation is consistent with phenomenological models (*52*, *53*) that predicted neutrino emission and absorption of gamma-ray photons in this source. Like the blazar TXS 0506+056 (*21*), the active galaxy NGC 1068 is a point source of high-energy neutrinos.

REFERENCES AND NOTES

1. J. Abraham *et al.*, *Nucl. Instrum. Methods Phys. Res. A* **523**, 50–95 (2004).
2. The Pierre Auger Collaboration, *Nucl. Instrum. Methods Phys. Res. A* **798**, 172–213 (2015).
3. T. Abu-Zayyad *et al.*, *Nucl. Instrum. Methods Phys. Res. A* **689**, 87–97 (2012).
4. S. R. Kelner, F. A. Aharonian, V. V. Bugayov, *Phys. Rev. D* **74**, 034018 (2006).
5. S. R. Kelner, F. A. Aharonian, *Phys. Rev. D* **78**, 034013 (2008).
6. A. De Angelis, G. Galanti, M. Roncadelli, *Mon. Not. R. Astron. Soc.* **432**, 3245–3249 (2013).
7. P. Padovani *et al.*, *Astron. Astrophys. Rev.* **25**, 2 (2017).
8. C. K. Seyfert, *Astrophys. J.* **97**, 28 (1943).
9. R. Antonucci, *Annu. Rev. Astron. Astrophys.* **31**, 473–521 (1993).
10. C. M. Urry, P. Padovani, *Publ. Astron. Soc. Pac.* **107**, 803 (1995).
11. D. Eichler, *Astrophys. J.* **232**, 106 (1979).
12. V. S. Berezinsky, V. L. Ginzburg, *Mon. Not. R. Astron. Soc.* **194**, 3–14 (1981).
13. K. Mannheim, P. L. Biermann, *Astron. Astrophys.* **221**, 211–220 (1989).
14. F. Halzen, E. Zas, *Astrophys. J.* **488**, 669–674 (1997).
15. M. G. Aartsen *et al.*, *J. Instrum.* **12**, P03012 (2017).
16. IceCube Collaboration, *Science* **342**, 1242856 (2013).
17. M. G. Aartsen *et al.*, *Phys. Rev. Lett.* **125**, 121104 (2020).
18. R. Abbasi *et al.*, *Phys. Rev. D* **104**, 022002 (2021).
19. M. G. Aartsen *et al.*, *Astropart. Phys.* **92**, 30–41 (2017).
20. IceCube Collaboration *et al.*, *Science* **361**, eaat1378 (2018).
21. IceCube Collaboration, *Science* **361**, 147–151 (2018).
22. P. Padovani, F. Oikonomou, M. Petropoulou, P. Giommi, E. Resconi, *Mon. Not. R. Astron. Soc.* **484**, L104–L108 (2019).
23. M. G. Aartsen *et al.*, *Phys. Rev. Lett.* **124**, 051103 (2020).
24. M. G. Aartsen *et al.*, *Eur. Phys. J. C* **79**, 234 (2019).
25. M. G. Aartsen *et al.*, *Astrophys. J.* **833**, 3 (2016).
26. Materials and methods are available as supplementary materials.
27. J. Ahrens *et al.*, *Nucl. Instrum. Methods Phys. Res. A* **524**, 169–194 (2004).
28. R. Abbasi *et al.*, *J. Instrum.* **16**, P08034 (2021).
29. R. Abbasi *et al.*, *Astropart. Phys.* **34**, 48–58 (2010).
30. T. K. Gaisser, R. Engel, E. Resconi, *Cosmic Rays and Particle Physics: Second Edition* (Cambridge Univ. Press, 2016).
31. M. Aartsen *et al.*, *Astrophys. J.* **835**, 151 (2017).
32. S. Abdollahi *et al.*, *Astrophys. J. Suppl. Ser.* **247**, 33 (2020).
33. S. P. Wakely, D. Horan, *International Cosmic Ray Conference*, vol. 3 of *International Cosmic Ray Conference* (2008), pp. 1341–1344.
34. P. Padovani *et al.*, *Mon. Not. R. Astron. Soc.* **480**, 192–203 (2018).
35. M. Bustamante, J. F. Beacom, W. Winter, *Phys. Rev. Lett.* **115**, 161302 (2015).
36. C. A. Argüelles, T. Katori, J. Salvado, *Phys. Rev. Lett.* **115**, 161303 (2015).
37. J. Bland-Hawthorn *et al.*, *Astrophys. Space Sci.* **248**, 9–19 (1997).
38. B. F. Madore, in *27th Rencontres de Moriond: Physics of Nearby Galaxies: Nature or Nurture?*, T. X. Thuan, J. Tran Thanh Van, C. Balkoski, Eds. (Ed. Frontieres, 1992), pp. 25–28.
39. Gravity Collaboration, O. Pfuhl *et al.*, *Astron. Astrophys.* **634**, A1 (2020).
40. M. Ajello *et al.*, *Astrophys. J.* **892**, 105 (2020).
41. S. Abdollahi *et al.*, *Astrophys. J. Suppl. Ser.* **247**, 33 (2020).
42. V. A. Acciari *et al.*, *Astrophys. J.* **883**, 135 (2019).
43. C. Ricci *et al.*, *Astrophys. J. Lett.* **815**, L13 (2015).
44. A. Marinucci *et al.*, *Mon. Not. R. Astron. Soc.* **456**, L94–L98 (2016).
45. A. Zaino *et al.*, *Mon. Not. R. Astron. Soc.* **492**, 3872–3884 (2020).
46. A. B. Romeo, K. Fathi, *Mon. Not. R. Astron. Soc.* **460**, 2360–2367 (2016).
47. B. Eichmann, J. B. Tjus, *Astrophys. J.* **821**, 87 (2016).
48. G. Cecil, J. Bland, R. B. Tully, *Astrophys. J.* **355**, 70 (1990).
49. R. Silberberg, M. M. Shapiro, *Neutrinos as a Probe for the Nature of and Processes in Active Galactic Nuclei*, vol. 10 of *16th International Cosmic Ray Conference*, S. Miyake, N. G. Kaigi, N. B. Gakkai, Eds. (Institute for Cosmic Ray Research, 1979), p. 357.
50. T. M. Yoast-Hull, J. S. Gallagher III, E. G. Zweibel, J. E. Everett, *Astrophys. J.* **780**, 137 (2014).
51. A. Lamastra *et al.*, *Astron. Astrophys.* **596**, A68 (2016).
52. Y. Inoue, D. Khangulyan, A. Doi, *Astrophys. J. Lett.* **891**, L33 (2020).
53. K. Murase, S. S. Kimura, P. Mészáros, *Phys. Rev. Lett.* **125**, 011101 (2020).
54. R. Silberberg, M. M. Shapiro, in *Composition and Origin of Cosmic Rays*, M. M. Shapiro, Ed., vol. 107 of *NATO Advanced Study Institute (ASI) Series C* (Springer, 1983), pp. 231–244.
55. Y. Inoue, D. Khangulyan, S. Inoue, A. Doi, *Astrophys. J.* **880**, 40 (2019).
56. F. W. Stecker, C. Done, M. H. Salamon, P. Sommers, *Phys. Rev. Lett.* **66**, 2697–2700 (1991).
57. R. Silberberg, M. M. Shapiro, C. H. Starr, in *Particle Astrophysics and Cosmology*, M. M. Shapiro, R. Silberberg, J. P. Wefel, Eds.,

vol. 394 of *NATO Advanced Study Institute (ASI) Series C* (Springer, 1993), p. 53.
58. K. Murase, E. Waxman, *Phys. Rev. D* **94**, 103006 (2016).
59. F. Capel, D. J. Mortlock, C. Finley, *Phys. Rev. D* **101**, 123017 (2020).
60. C. F. Tung *et al*., *J. Open Source Softw.* **6**, 3194 (2021).
61. G. Paturel *et al*., *Astron. Astrophys.* **412**, 45–55 (2003).

ACKNOWLEDGMENTS

We dedicate this work to our recently deceased colleagues, Thomas K. Gaisser and P. Buford Price. The IceCube Collaboration acknowledges contributions to this manuscript from H. Niederhausen and T. Glauch. **Funding:** The authors gratefully acknowledge support from the following agencies and institutions. USA: US National Science Foundation–Office of Polar Programs, US National Science Foundation–Physics Division, US National Science Foundation–EPSCoR, Wisconsin Alumni Research Foundation, Center for High Throughput Computing (CHTC) at the University of Wisconsin–Madison, Open Science Grid (OSG), Extreme Science and Engineering Discovery Environment (XSEDE), the Frontera computing project at the Texas Advanced Computing Center, US Department of Energy–National Energy Research Scientific Computing Center, the Particle Astrophysics research computing center at the University of Maryland, Institute for Cyber-Enabled Research at Michigan State University, and the astroparticle physics computational facility at Marquette University. Belgium: Funds for Scientific Research (FRS-FNRS and FWO), FWO Odysseus and Big Science programs, and Belgian Federal Science Policy Office (Belspo). Germany: Bundesministerium für Bildung und Forschung (BMBF), Deutsche Forschungsgemeinschaft (DFG), Helmholtz Alliance for Astroparticle Physics (HAP), Initiative and Networking Fund of the Helmholtz Association, Deutsches Elektronen Synchrotron (DESY), and the High Performance Computing cluster of the RWTH Aachen. Sweden: Swedish Research Council, Swedish Polar Research Secretariat, Swedish National Infrastructure for Computing (SNIC), and Knut and Alice Wallenberg Foundation. Australia: Australian Research Council. Canada: Natural Sciences and Engineering Research Council of Canada, Calcul Québec, Compute Ontario, Canada Foundation for Innovation, WestGrid, and Compute Canada. Denmark: Villum Fonden and Carlsberg Foundation. New Zealand: Marsden Fund. Japan: Japan Society for Promotion of Science (JSPS) and Institute for Global Prominent Research (IGPR) of Chiba University. Korea: National Research Foundation of Korea (NRF). Switzerland: Swiss National Science Foundation (SNSF). UK: the Department of Physics of the University of Oxford. **Author contributions:** The IceCube Collaboration designed, constructed, and now operates the IceCube Neutrino Observatory. Data processing and calibration, Monte Carlo simulations of the detector and of theoretical models, and data analyses were performed by a large number of collaboration members, who also discussed and approved the scientific results presented here. The manuscript was reviewed by the entire collaboration before publication, and all authors approved the final version. Contributions listed below are in the following areas: (a) Conceptualization, formal analysis, and methodology; (b) Data curation and resources; (c) Funding acquisition and project administration; (d) Investigation; (e) Software; (f) Supervision; (g) Validation; (h) Writing – original draft and visualization; and (i) Writing – review and editing. Specific contributions are as follows: R. Abbasi (d), M. Ackermann (d), J. Adams (c, d), J. A. Aguilar (c, d), M. Ahlers (d), M. Ahrens (d), J. M. Alameddine (d, e), A. A. Alves Jr. (d), N. M. Amin (d), K. Andeen (b, c, d), G. Anton (c, d), C. Argüelles (b, d), Y. Ashida (d), S. Axani (b, d, e), X. Bai (b, c, e), A. Balagopal V. (d), B. Bastian (d), V. Basu (d), S. Baur (d), J. J. Beatty (d), K.-H. Becker (d), J. Becker Tjus (c), C. Bellenghi (a, b, e, g, h, i), S. BenZvi (b, c, d, i), D. Berley (c), E. Bernardini (d), D. Bindig (d), E. Blaufuss (b, c, d, e, i), S. Blot (d, i), F. Bontempo (d), J. Borowka (g, i), S. Böser (c, d), O. Botner (a, b, c, d, i), J. Böttcher (b, e, g, i), E. Bourbeau (d), F. Bradascio (d), J. Braun (b, d, e), J. Brostean-Kaiser (d), S. Browne (d), A. Burgman (d), R. T. Burley (d), R. S. Busse (d), M. A. Campana (d), E. G. Carnie-Bronca (d), C. Chen (d), D. Chirkin (b, d, e), B. A. Clark (b, d, e, i), L. Classen (d), A. Coleman (b, d, e), G. H. Collin (b, d, e), J. M. Conrad (b, c, d), P. Coppin (d), P. Correa (d), R. Cross (b, d), C. Dappen (b, g, i), P. Dave (d), C. De Clercq (d), J. J. DeLaunay (d), D. Delgado López (d), H. Dembinski (b, d, e), K. Deoskar (d), A. Desai (d), P. Desiati (b, c, d, e), K. D. de Vries (d), G. de Wasseige (d), T. DeYoung (b, c, d), A. Diaz (b, d, e), J. C. Díaz-Vélez (b, d, e), M. Dittmer (d), H. Dujmovic (d), M. A. DuVernois (b, d), E. Dvorak (b, e), T. Ehrhardt (b, d), P. Eller (b, e, i), R. Engel (c), H. Erpenbeck (b, g, i), J. Evans (d), P. A. Evenson (b, d), K. L. Fan (d, e), A. Fedynitch (d), N. Feigl (d), S. Fiedlschuster (d), C. Finley (a, c, d, i), L. Fischer (d), A. Franckowiak (d), E. Friedman (b, d, e), A. Fritz (d), P. Fürst (b, e, g, i), T. K. Gaisser (a, b, c, d), E. Ganster (b, e, g, i), A. Garcia (d), S. Garrappa (d), L. Gerhardt (d), C. Glaser (c, d), T. Glauch (a, b, c, d, e, f, g, h, i), T. Glüsenkamp (d), A. Goldschmidt (d), J. G. Gonzalez (b, c, d, e), D. Grant (c, d, i), S. Griswold (b, d), C. Günther (g, i), P. Gutjahr (d), C. Haack (a, b, e, f, g, h), A. Hallgren (a, b, c, d), R. Halliday (b, d), L. Halve (g, i), F. Halzen (a, b, c, d, e, h, i), M. Ha Minh (e, i), K. Hanson (b, c, d, e), J. Hardin (b, d, e), A. A. Harnisch (d, e), A. Haungs (c, d), K. Helbing (d), F. Henningsen (e, i), S. Hickford (d), C. Hill (d), G. C. Hill (a, b, c, d), K. D. Hoffman (c, d), R. Hoffmann (d), K. Hoshina (b, d, e), M. Huber (a, e), T. Huber (d), K. Hultqvist (c, d), M. Hünnefeld (d), R. Hussain (b, d, e), K. Hymon (d), S. In (d), N. Iovine (d), A. Ishihara (d, e), M. Jansson (d), M. Jeong (d), M. Jin (d), B. J. P. Jones (b, c, d, e), D. Kang (d), W. Kang (d), X. Kang (d), A. Kappes (c, d), D. Kappesser (d), L. Kardum (d), T. Karg (d), M. Karl (a, e, i), A. Karle (a, b, c, d, e, i), U. Katz (c, d), M. Kauer (b, d, e), M. Kellermann (g, i), J. L. Kelley (b, c, d, e), A. Kheirandish (d, i), K. Kin (d), T. Kintscher (d), S. R. Klein (c, d), R. Koirala (d), H. Kolanoski (d), T. Kontrimas (a, b, e, g, h, i), L. Köpke (a, c, d), C. Kopper (b, c, e, f, i), D. J. Koskinen (d), P. Koundal (d), M. Kovacevich (d), M. Kowalski (d), T. Kozynets (d), N. Kurahashi (b, c, d, e), N. Lad (d), C. Lagunas Gualda (d), M. J. Larson (b, c, d, e), F. Lauber (d), J. P. Lazar (b, d), K. Leonard (b, d, e), A. Leszczyńska (d), Q. R. Liu (b, d, e), E. Lohfink (d), C. J. Lozano Mariscal (d), L. Lu (b, d, e), F. Lucarelli (a, b), A. Ludwig (e), W. Luszczak (b, d, e), Y. Lyu (d), W. Y. Ma (d), J. Madsen (c, d, e), Y. Makino (b, d), S. Mancina (b, d, e), I. C. Mariş (d), I. Martinez-Soler (d), K. Mase (e), F. McNally (d), J. V. Mead (d), K. Meagher (b, d, e), S. Mechbal (d), A. Medina (d, e), M. Meier (d), S. Meighen-Berger (e, i), J. Micallef (d, e), D. Mockler (d), T. Montaruli (a, b, c, d, e, f, i), R. Morse (a, b, c, d, e), M. Moulai (b, d, e), R. Naab (d), R. Nagai (d), U. Naumann (d), J. Necker (d), H. Niederhausen (a, b, c, d, e, f, g, h, i), M. U. Nisa (d), S. C. Nowicki (d), A. Obertacke Pollmann (d), M. Oehler (d), A. Olivas (b, c, d, e), E. O'Sullivan (c, d), H. Pandya (d), N. Park (a, d, i), G. K. Parker (b, d, e), E. N. Paudel (d), L. Paul (b, d), C. Pérez de los Heros (a, b, c, d), L. Peters (b, g, i), S. Philippen (a, b, e, g, i), S. Pieper (d), A. Pizzuto (b, c, d, e), M. Plum (b, d), Y. Popovych (d), M. Prado Rodriguez (b, c, d, e), C. Raab (d), J. Rack-Helleis (d), K. Rawlins (b, c, d, e), A. Rehman (d), R. Reimann (a, b, e, g, i), G. Renzi (d), E. Resconi (a, b, c, f, h), S. Reusch (d), W. Rhode (c, d), B. Riedel (b, c, d, e), E. J. Roberts (d), S. Robertson (d), G. Roellinghoff (d), M. Rongen (c, d), C. Rott (d), T. Ruhe (c, d), D. Ryckbosch (c, d), D. Rysewyk Cantu (d), I. Safa (b, d, e), J. Saffer (d), S. E. Sanchez Herrera (d), A. Sandrock (d, e), J. Sandroos (d), M. Santander (c, d, i), S. Sarkar (Oxford U.) (d), K. Satalecka (d), M. Schaufel (g, i), H. Schieler (d), S. Schindler (d), T. Schmidt (b, d, e), A. Schneider (b, d, e), J. Schneider (d), F. G. Schröder (b, c, d), L. Schumacher (a, b, e, f, i), G. Schwefer (g, i), S. Sclafani (b, d), D. Seckel (a, b, c, d), S. Seunarine (d), A. Sharma (d), S. Shefali (d), M. Silva (b, d, e), B. Skrzypek (d), B. Smithers (b, d, e), R. Snihur (b, d, e), J. Soedingrekso (d, e), D. Soldin (b, c, d, e), C. Spannfellner (i), G. M. Spiczak (d), C. Spiering (d), J. Stachurska (d), M. Stamatikos (d), T. Stanev (a, d), R. Stein (d), J. Stettner (a, b, e, g, i), A. Steuer (d), R. Stokstad (a, c, d), T. Stürwald (d), T. Stuttard (b, e), G. W. Sullivan (b, c, d), I. Taboada (c, d, i), S. Tilav (a, b, c, d, e, g), F. Tischbein (g, i), K. Tollefson (d), C. Tönnis (d), S. Toscano (d), D. Tosi (b, d, e), A. Trettin (d), M. Tselengidou (d), C. F. Tung (d), A. Turcati (a, e), R. Turcotte (d), J. P. Twagirayezu (d), M. A. Unland Elorrieta (d), N. Valtonen-Mattila (b, d), J. Vandenbroucke (b, c, d, e, h, i), N. Van Eijndhoven (c, d), D. Vannerom (d, e), J. van Santen (d), C. Walck (d), C. Weaver (b, d, e), P. Weigel (d, e), A. Weindl (b), J. Weldert (d), C. Wendt (b, c, d, e), J. Werthebach (d), M. Weyrauch (d), N. Whitehorn (c, d, e, i), C. H. Wiebusch (a, c, f, g, i), D. R. Williams (c, d), M. Wolf (a, b, c, d, e, f, g, h), G. Wrede (d), J. Wulff (e, g), S. Yoshida (d, e), S. Yu (d), T. Yuan (b, c, d, e), and P. Zhelnin (d). **Competing interests:** There are no competing interests to declare. **Data and materials availability:** Numerical results for all 110 sources are listed in table S3. All data and software used in this paper, including the event list and analysis scripts, are available from the IceCube data archive at https://icecube.wisc.edu/science/data/neutrino-emission-from-ngc-1068.

SUPPLEMENTARY MATERIALS

science.org/doi/10.1126/science.abg3395
Materials and Methods
Supplementary Text
Figs. S1 to S30
Tables S1 to S4
IceCube Collaboration Author List
References (*62*–*98*)

Submitted 19 November 2021; accepted 22 September 2022
10.1126/science.abg3395